THE JOURNAL OF PHYSICAL CHEMISTRY A
A JOURNAL OF THE AMERICAN CHEMICAL SOCIETY

pubs.acs.org/JPCA

Article

Revisiting the Spin−Lattice Relaxation of Homonuclear In-Phase and Antiphase NMR Magnetization

Lauren M. Kehoe, Zachary G. Mayes, Kelsey E. Brakensiek, Emma L. Ellis, Adam J. Alderfer, Lingyu Chi, and Klaus Woelk*

Cite This: https://doi.org/10.1021/acs.jpca.5c05247

Read Online

ACCESS | Metrics & More | Article Recommendations

ABSTRACT: Hyperpolarization techniques such as dynamic nuclear polarization (DNP), chemically-induced dynamic nuclear polarization (CIDNP), and parahydrogen-induced polarization (PHIP) enhance the sensitivity of NMR spectroscopy and MRI, but the associated antiphase magnetization patterns often relax faster than those of conventional in-phase signals. This study analyzes the spin−lattice relaxation matrix for single-quantum transitions in an isolated, weakly coupled two-spin AX system to identify eigenvectors and eigenvalues that govern the time evolution of in-phase and antiphase longitudinal magnetization. The analysis predicts that AX antiphase magnetization, such as that generated by PHIP hydrogenations in high magnetic field, can relax up to twice as fast as the in-phase magnetization of traditional inversion-recovery or saturation-recovery experiments. To validate these predictions, a dedicated NMR pulse sequence was used to selectively generate and monitor antiphase magnetization. *trans*-Cinnamic acid in deuterated DMSO served as a model compound, with the hydrogen atoms on its central conjugated double bond forming a weakly coupled AX spin system with a large scalar coupling (>16 Hz). The large scalar coupling allowed for the separate integration of the two lines in each doublet. Experimental results confirm an accelerated relaxation of antiphase magnetization but also reveal that in-phase relaxation is influenced by double-quantum transitions, which do not contribute to the relaxation of antiphase magnetization. The findings of this study highlight the importance of distinguishing in-phase from antiphase relaxation, providing a basis for optimizing hyperpolarization experiments with explicit consideration of antiphase signal dynamics.

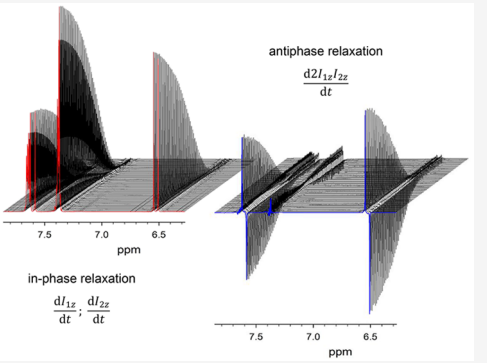

INTRODUCTION

Nuclear magnetic resonance (NMR) spectroscopy is a widely employed analytical technique to determine molecular structure, investigate chemical environments, and study dynamic processes in both solution and solid phases. The spin-physics principles underlying NMR also form the basis for magnetic resonance imaging (MRI), where spatial encoding of spin populations enables noninvasive, high-resolution imaging for clinical diagnostics including tumor detection and tissue characterization. A principal limitation of both NMR and MRI, however, is their inherently low sensitivity, which stems from the small population differences between nuclear spin states at thermal equilibrium under conventional magnetic field strengths.

To overcome this limitation, a variety of nuclear spin hyperpolarization techniques have been developed to transiently enhance spin polarization well beyond thermal equilibrium values.[1,2] Spin hyperpolarization involves the intentional redistribution of spin populations, resulting in an overpopulation of certain energy levels and a corresponding depletion of others. These non-Boltzmann population distributions can lead to significantly enhanced NMR signal intensities, often by several orders of magnitude, and improved image contrast in MRI applications.

Once hyperpolarization is achieved, the perturbed spin system relaxes back to thermal equilibrium through spin−lattice interactions. This process is commonly quantified by the longitudinal relaxation time constant T_1, which depends on factors such as local magnetic field fluctuations, molecular motion, and spin−spin couplings. The time constant T_1 ultimately defines the time window during which hyperpolarized spin states can be effectively exploited. For hyperpolarization methods to be successful, polarization buildup must occur on a time scale that is faster than T_1 relaxation.

In systems where spin hyperpolarization involves coupled nuclear spins, such as in parahydrogen-induced polarization

Received: July 28, 2025
Revised: September 10, 2025
Accepted: September 11, 2025

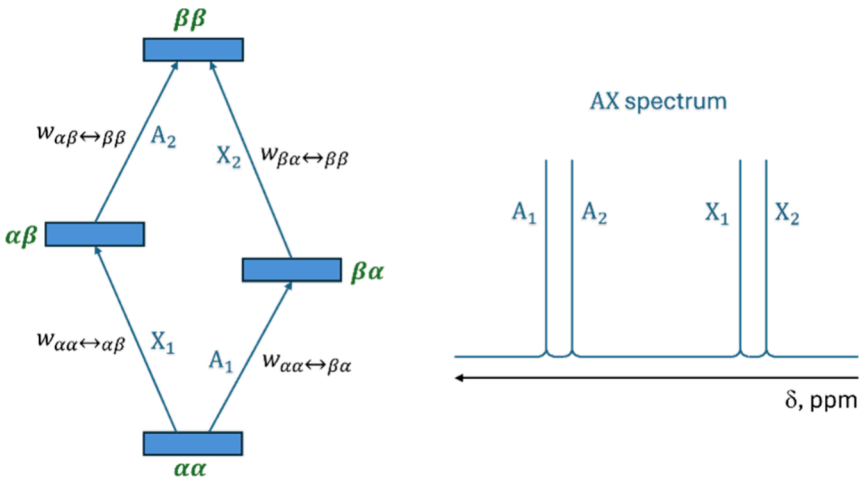

Figure 1. Homonuclear spin energy levels (left) of a weakly coupled two-spin system (AX).[10] The single-quantum transitions (A_1, A_2, X_1, and X_2) (indicated by arrows) correspond to the observable NMR signals shown schematically in the AX spectrum (right). If the transition probabilities $w_{\alpha\alpha\leftrightarrow\beta\alpha}$, $w_{\alpha\alpha\leftrightarrow\beta\alpha}$, $w_{\alpha\alpha\leftrightarrow\beta\alpha}$, and $w_{\alpha\alpha\leftrightarrow\beta\alpha}$ are identical, then the resulting spectrum under thermodynamic equilibrium conditions will exhibit equal-intensity signals for all four transitions.

(PHIP)[2−6] or the multiplet effect observed in chemically-induced dynamic nuclear polarization (CIDNP),[7] spin−lattice relaxation is often estimated by the same T_1 value that is measured with inversion-recovery, saturation-recovery, or related pulse protocols.[8,9] However, the population distribution in hyperpolarized coupled nuclear spin systems can lead to dramatically different relaxation dynamics, even though the individual transitions and their probabilities may not change.

The relaxation kinetics of spin population redistribution in coupled nuclear spin systems, whether initiated by inversion, recovery, spin hyperpolarization, or other perturbation techniques, can be described using relaxation matrices composed of coupled first-order differential equations. Eigenvalue decomposition of such matrices reveals a set of eigenvectors, each associated with a distinct relaxation mode and decay rate. Inversion-recovery and saturation-recovery experiments typically probe a single slowly relaxing eigenmode, whereas hyperpolarized spin systems frequently involve additional eigenmodes that decay more rapidly.

THEORY OF RELAXATION IN A WEAKLY COUPLED TWO-SPIN SYSTEM

A system consisting of two weakly coupled spin-1/2 nuclei gives rise to four distinct energy levels, associated with the spin-state combinations $\alpha\alpha$, $\beta\alpha$, $\alpha\beta$, and $\beta\beta$, where α denotes a spin aligned with the external magnetic field and β a spin aligned against the field.[9] As illustrated in Figure 1, these energy levels permit four single-quantum transitions, each not only contributing to observable signals in the NMR spectrum but also representing distinct relaxation pathways. The probability of population exchange between two adjacent spin states is described by a transition probability $w_{i\leftrightarrow j}$, where subscript indices identify the pair of spin states involved. For example, the probability $w_{\alpha\alpha\leftrightarrow\beta\alpha}$ corresponds to the transition between the values of $\alpha\alpha$ and $\beta\alpha$. As these transition probabilities are bidirectional, notation throughout this work consistently lists the lower-energy state first.

In a first-order approximation, relaxation contributions from double-quantum transitions (e.g., $w_{\alpha\alpha\leftrightarrow\beta\beta}$) and zero-quantum transitions (e.g., $w_{\beta\alpha\leftrightarrow\alpha\beta}$) are neglected. Under this assumption, population redistribution following a perturbation from nuclear spin equilibrium proceeds exclusively via single-quantum transitions between adjacent energy levels. The resulting time-dependent population dynamics is therefore governed by the following set of differential equations:[11]

$$\frac{d[\beta\beta]}{dt} = w_{\alpha\beta\leftrightarrow\beta\beta}([\alpha\beta] - [\beta\beta]) + w_{\beta\alpha\leftrightarrow\beta\beta}([\beta\alpha] - [\beta\beta]) \quad (1a)$$

$$\frac{d[\alpha\beta]}{dt} = w_{\alpha\beta\leftrightarrow\beta\beta}([\beta\beta] - [\alpha\beta]) + w_{\alpha\alpha\leftrightarrow\alpha\beta}([\alpha\alpha] - [\alpha\beta]) \quad (2a)$$

$$\frac{d[\beta\alpha]}{dt} = w_{\beta\alpha\leftrightarrow\beta\beta}([\beta\beta] - [\beta\alpha]) + w_{\alpha\alpha\leftrightarrow\beta\alpha}([\alpha\alpha] - [\beta\alpha]) \quad (3a)$$

$$\frac{d[\alpha\alpha]}{dt} = w_{\alpha\alpha\leftrightarrow\alpha\beta}([\alpha\beta] - [\alpha\alpha]) + w_{\alpha\alpha\leftrightarrow\beta\alpha}([\beta\alpha] - [\alpha\alpha]) \quad (4a)$$

Here, in analogy to concentration terms used in chemical kinetics, square brackets denote the populations of the individual spin states. More precisely, these quantities represent deviations from thermodynamic equilibrium populations. The system of eqs 1a to 4a provides a general kinetic framework for modeling spin−lattice relaxation in weakly coupled two-spin systems, forming the basis for further simplifications and matrix-based treatments.

Assuming equal transition probabilities for all single-quantum transitions, a common approximation in weakly coupled, homonuclear two-spin systems, each $w_{i\leftrightarrow j}$ can be replaced by a common rate constant w_1, where subscript 1 denotes single-quantum relaxation. Under this assumption, the rate eqs 1a to 4a simplify to

$$\frac{d[\beta\beta]}{dt} = w_1([\alpha\beta] + [\beta\alpha] - 2[\beta\beta]) \quad (1b)$$

$$\frac{d[\alpha\beta]}{dt} = w_1([\beta\beta] + [\alpha\alpha] - 2[\alpha\beta]) \quad (2b)$$

$$\frac{d[\beta\alpha]}{dt} = w_1([\beta\beta] + [\alpha\alpha] - 2[\beta\alpha]) \quad (3b)$$

https://doi.org/10.1021/acs.jpca.5c05247
J. Phys. Chem. A XXXX, XXX, XXX−XXX

$$\frac{d[\alpha\alpha]}{dt} = w_1([\alpha\beta] + [\beta\alpha] - 2[\alpha\alpha]) \tag{4b}$$

This system of coupled first-order differential equations can be expressed in matrix form as

$$\frac{d\mathbf{P}}{dt} = w_1 \cdot \mathbf{R} \cdot \mathbf{P} \tag{5}$$

where

$$\mathbf{P} = \begin{bmatrix} [\beta\beta] \\ [\alpha\beta] \\ [\beta\alpha] \\ [\alpha\alpha] \end{bmatrix}, \mathbf{R} = \begin{bmatrix} -2 & 1 & 1 & 0 \\ 1 & -2 & 0 & 1 \\ 1 & 0 & -2 & 1 \\ 0 & 1 & 1 & -2 \end{bmatrix}$$

The relaxation matrix **R** has four eigenvalues: 0, −2 (twice degenerate), and −4. These eigenvalues, combined with the rate constant w_1, represent characteristic relaxation rates, while the associated eigenvectors (shown in Figure 2) define spin population modes that evolve independently over time. These eigenvectors form an orthogonal basis for describing any nonequilibrium spin-state population and define distinct relaxation pathways with unique decay rates.

The eigenvector associated with the zero eigenvalue $[1\ 1\ 1\ 1]^T$ (Figure 2a) corresponds to the equilibrium state, in which all four spin states are populated according to Boltzmann equilibrium, and no further relaxation occurs. The eigenvector $[1\ 0\ 0\ -1]^T$ (Figure 2b), associated with eigenvalue −2, represents the relaxation pathway typically observed in inversion-recovery or saturation-recovery experiments. This mode reflects an overpopulation of the highest-energy level ($\beta\beta$) and a corresponding underpopulation in the lowest-energy state ($\alpha\alpha$), relative to equilibrium. A second eigenvector, $[0\ 1\ -1\ 0]^T$ (Figure 2c), also associated with eigenvalue −2, involves a differential population between the intermediate spin states, with overpopulation in $\alpha\beta$ and underpopulation in $\beta\alpha$. In contrast, the eigenvector $[1\ -1\ -1\ 1]^T$ (Figure 2d), associated with eigenvalue −4, represents a relaxation mode that decays twice as fast as the −2 modes. This fast-relaxing mode is characterized by an excess population in the outer states ($\beta\beta$ and $\alpha\alpha$) along with depletion in the intermediate states ($\alpha\beta$ and $\beta\alpha$).

According to the matrix formulation described above, relaxation following standard inversion-recovery or saturation-recovery excitation involves a single eigenmode with an eigenvalue of −2. The time constant associated with this decay is what is conventionally referred to as T_1. Within the matrix framework, this time constant is directly related to the transition probability w by the expression $T_1 = (2w)^{-1}$,[12] where the factor of 2 reflects the relaxation mode's eigenvalue.

Hyperpolarized spin systems, such as those generated via PHIP or observed through the multiplet effect in CIDNP, frequently exhibit initial population distributions that project significantly onto the −4 eigenmode.[1,7] In such cases, relaxation toward equilibrium is dominated by a faster decay component characterized by the eigenvalue −4, corresponding to a relaxation time constant of $(4w)^{-1}$. This mode proceeds at twice the rate of the conventional T_1 relaxation process, leading to a rapid loss of nonequilibrium spin order and a substantial reduction in the effective lifetime of hyperpolarized states. As a result, hyperpolarized systems often relax much faster than those predicted by standard inversion-recovery or

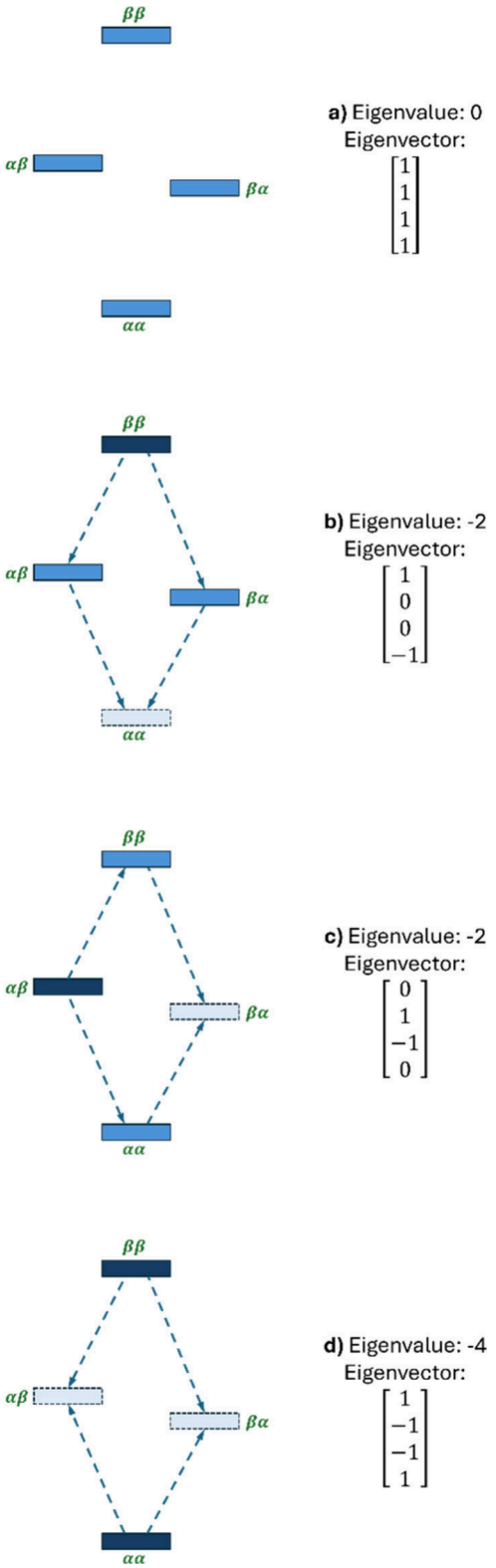

Figure 2. Spin-state population modes and associated eigenvectors for a weakly coupled two-spin (AX) system. Dark shading indicates overpopulation relative to thermal equilibrium, whereas light shading with dashed outlines denotes depletion. Blue dashed arrows indicate the single-quantum transitions between the four energy levels ($\beta\beta$, $\alpha\beta$, $\beta\alpha$, and $\alpha\alpha$) that mediate relaxation between adjacent levels. Each panel illustrates a distinct eigenmode of the relaxation matrix: (a) thermodynamic equilibrium (eigenvalue 0), (b) population excess in $\beta\beta$ and depletion in $\alpha\alpha$ (eigenvalue −2), (c) population excess in $\alpha\beta$

https://doi.org/10.1021/acs.jpca.5c05247
J. Phys. Chem. A XXXX, XXX, XXX−XXX

Figure 2. continued

and depletion in $\beta\alpha$ (eigenvalue −2), and (d) population excess in $\beta\beta$ and $\alpha\alpha$ with depletion in $\alpha\beta$ and $\beta\alpha$ (eigenvalue −4).

saturation-recovery measurements. Accurate interpretation of relaxation behavior in these systems therefore necessitates accounting for the full spectrum of contributing eigenmodes and their associated time constants. Notably, an early observation of unusually rapid relaxation in parahydrogen-induced polarization (PHIP) experiments was already reported in the 1988 Master's thesis (Diplomarbeit) of one of the present authors.[13] In that study, catalytic hydrogenation of acetonitrile with enriched parahydrogen produced hyperpolarized propionitrile, which exhibited longitudinal spin relaxation more than twice as fast as the T_1 time measured by conventional inversion-recovery on the same solution after a full return to equilibrium. At the time, this effect was attributed to enhanced relaxation caused by reactive intermediates or nuclear Overhauser effects. Only in retrospect is this behavior interpreted as a manifestation of relaxation through faster eigenmodes.

EXPERIMENTAL SECTION

trans-Cinnamic acid was used as a model compound for investigating the relaxation dynamics in a weakly coupled homonuclear two-spin system. The *trans*-vicinal protons at the central conjugated double bond (H_A and H_X in Figure 3)

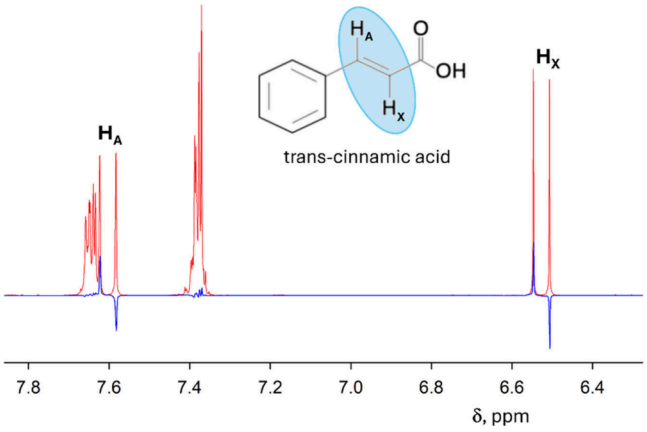

Figure 3. Standard one-dimensional 400 MHz ^{1}H NMR spectrum (red trace) of (2*E*)-3-phenylprop-2-enoic acid (commonly known as *trans*-cinnamic acid) in deuterated dimethyl sulfoxide (DMSO-d_6). The *trans*-vicinal protons H_A and H_X at the central conjugated double bond form a weakly coupled AX spin system with a large scalar coupling (J = 16.04 Hz), giving rise to two well-resolved doublets at 7.60 ppm (H_A) and 6.53 ppm (H_X). The multiplets centered around 7.64 and 7.37 ppm arise from the aromatic protons. The blue trace shows signals derived following the generation of longitudinal antiphase magnetization ($2I_{1z}I_{2z}$), which corresponds to an eigenmode population characterized by eigenvalue −4 (Figure 2d).

exhibit a scalar coupling constant (J = 16.04 Hz) that ranks among the largest reported for an isolated, coupled two-spin system. Under the high field strength of a superconducting NMR magnet, these protons form an AX spin system, characterized by a chemical shift difference of 1.34 ppm, which exceeds the coupling constant by more than an order of magnitude (e.g., 536 Hz at 400 MHz). AX systems of this type yield two well-resolved doublets in the proton NMR spectrum, corresponding to the single-quantum transitions illustrated in Figure 1. The large scalar coupling allows for the separate integration of the two lines in each doublet.

Conventional spin−lattice relaxation of these protons (H_A and H_X in Figure 3) was determined using the recently introduced split-inversion pulse and recovery (SIP-R) protocol, a modified dual-scan inversion-recovery experiment that converts the traditional rise-to-maximum relaxation behavior into a decay-to-zero functionality.[14,15] This reformulation reduces the dependent variables that must be optimized in an exponential curve fit from three to two and yields relaxation curves that are more amenable to numerical inverse Laplace transform (ILT) algorithms,[16,17] which are commonly employed to resolve multiexponential relaxation components in systems with overlapping kinetic processes.

To isolate and selectively observe the relaxation of spin populations associated with the eigenmode corresponding to eigenvalue −4, a dedicated NMR pulse sequence (Figure 4)

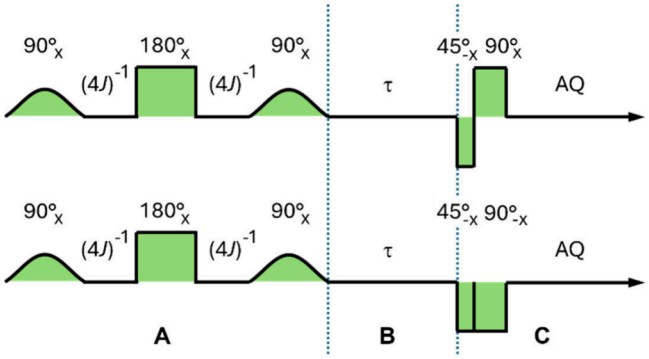

Figure 4. Dual-scan NMR pulse sequences designed to isolate and monitor relaxation of spin populations associated with the fast-relaxing eigenmode (eigenvalue −4) in a weakly coupled two-spin system. The sequence consists of three segments: (A) generation of $2I_{1z}I_{2z}$ longitudinal two-spin order from thermal equilibrium via frequency-selective 90° pulses and scalar coupling evolution time with a central 180° refocusing pulse; (B) a variable relaxation delay τ allowing for spin−lattice relaxation; and (C) the selective detection of remaining $2I_{1z}I_{2z}$ spin order using an effective 45° pulse in the first scan and an effective −135° pulse in the second scan. The combined result of the two scans converts the longitudinal two-spin order into observable single-quantum coherence while simultaneously suppressing contributions from pre-existing single-quantum coherence. Selective pulses are applied at the resonance frequencies of either nucleus A or X. Subscript indices denote the transmitter phases of each pulse, and AQ marks the acquisition period.

was developed consisting of three segments (A, B, and C). In Part A, spin-state populations reflecting the eigenvector of eigenvalue −4 (Figure 2d) are generated from thermal equilibrium. Part B introduces a variable delay period to allow for spin−lattice relaxation. In Part C, the residual eigenmode population is selectively detected, allowing direct measurement of the relaxation behavior specific to this fast-relaxing mode.

Within the framework of product operator formalism, the eigenmode associated with eigenvalue −4 corresponds to longitudinal antiphase coherence, represented by the non-classical two-spin operator $2I_{1z}I_{2z}$.[18,19] In this operator, I denotes spin polarization (i.e., the population difference between the α and β spin states), and subscripts identify the

https://doi.org/10.1021/acs.jpca.5c05247
J. Phys. Chem. A XXXX, XXX, XXX−XXX

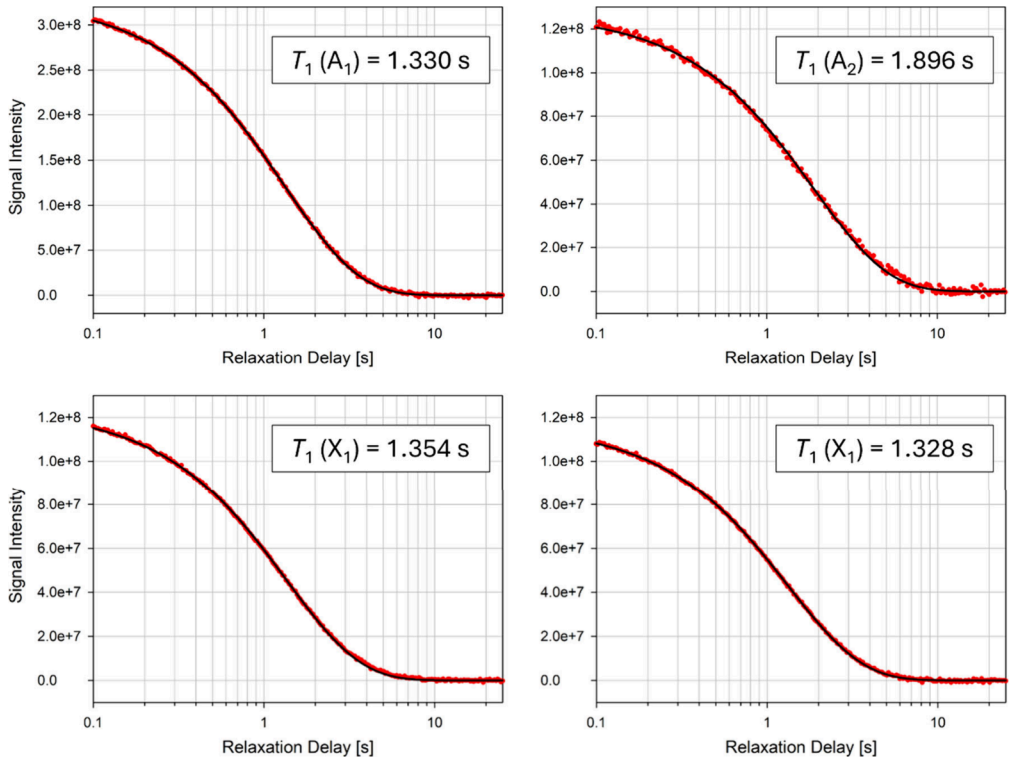

Figure 5. Relaxation plots of in-phase signal intensities of the *trans*-cinnamic acid *trans*-vicinal protons (H_A and H_X) as a function of relaxation delay. The ^{1}H NMR signals were obtained by SIP-R inversion-recovery experiments and integrated over a 16 Hz (0.04 ppm) range centered around each resonance. Shown are relaxation plots for A_1, A_2, X_1, and X_2 (as defined in Figure 1). The experimental data (red circles) are overlaid with monoexponential fits (black lines), from which the relaxation time constants T_1 were extracted. The about 2.5 times larger intensity observed for A_1 arises from partial overlap with aromatic proton signals.

individual nuclei in the coupled spin system; the Cartesian index z refers to the axis aligned with the static magnetic field in the rotating frame. Such a $2I_{1z}I_{2z}$ spin order can be generated from thermal equilibrium magnetization without employing hyperpolarization techniques. It is established through a pulse sequence (Part A in Figure 4) that begins with the frequency-selective excitation[20] of one of the coupled nuclei, followed by a mixing period during which antiphase coherence evolves under the influence of scalar coupling. A second frequency-selective pulse, applied to the same nucleus, then converts this antiphase coherence into the desired longitudinal two-spin order.[18] Frequency-selective excitation was performed using a $\sin(x)/x$-shaped radiofrequency pulse (sinc pulse) of 1000 discrete intensity steps truncated before and after the first zero crossings. The sinc pulse duration was adjusted to 20 ms to achieve an excitation bandwidth of 100 Hz around the center of the H_X doublet at 6.53 ppm (Figure 3). The performance of the sinc pulse was optimized by varying the pulse power until the maximum intensity was recorded for signals within the excitation bandwidth. Only H_X resonances were selectively excited because their chemical shift is well separated from other resonances of *trans*-cinnamic acid, unlike that of H_A, which overlaps with resonances from the aromatic protons. After selective excitation of one of the *trans*-vicinal protons, scalar coupling transfers coherence between the coupled spins, leading to antiphase signals for both H_A and H_X.

A nonselective 180° pulse at the midpoint of the mixing period serves to refocus the antiphase coherence along the negative axis of the initial excitation, enhancing the efficiency of the following transfer to $2I_{1z}I_{2z}$ longitudinal spin order. Optimal evolution of the two-spin order occurs when the total mixing time is set to $(2J)^{-1}$, implemented here as two intervals of $(4J)^{-1}$ before and after the 180° refocusing pulse. For *trans*-cinnamic acid, where the scalar coupling constant between the *trans*-vicinal protons is J = 16.04 Hz, the mixing delays were set to $(4J)^{-1}$ = 15.6 ms.

To selectively detect the $2I_{1z}I_{2z}$ spin order, a dual-scan acquisition strategy is employed, as shown in Part C of Figure 4. This detection scheme uses a pair of effective pulses: one with a nominal flip angle of +45° and the other with −135°. Two-spin orders such as $2I_{1z}I_{2z}$ exhibit twice the Rabi frequency (nutation frequency) compared to their single-spin operators $(I_{1z} + I_{2z})$.[21,22] As a result, the paired pulses act effectively as +90° and −270° excitations for the two-spin order, reinforcing its detection when the signals from the two scans are added. In contrast, for single-spin orders, the 45° and −135° pulses yield opposing transverse contributions that cancel upon coaddition, thereby suppressing any pre-existing single-quantum coherence. In practice, the pulse widths used in this detection block were empirically optimized by executing Part C of the dual-scan experiment in isolation and minimizing the detection of *trans*-cinnamic acid signals under thermal equilibrium conditions. A spectrum recorded by the dual-scan method (Figure 4), using the optimized pulse widths and a minimum relaxation delay of 0.1 s, is shown as the blue trace in Figure 3 and compared to the standard *trans*-cinnamic acid spectrum.

Figures 5 and 6 show relaxation curves obtained from integrated signal intensities of the *trans*-vicinal protons (H_A and H_X) in the spectrum of *trans*-cinnamic acid in DMSO-d_6. Figure 5 displays the relaxation of the in-phase signals acquired

https://doi.org/10.1021/acs.jpca.5c05247
J. Phys. Chem. A XXXX, XXX, XXX−XXX

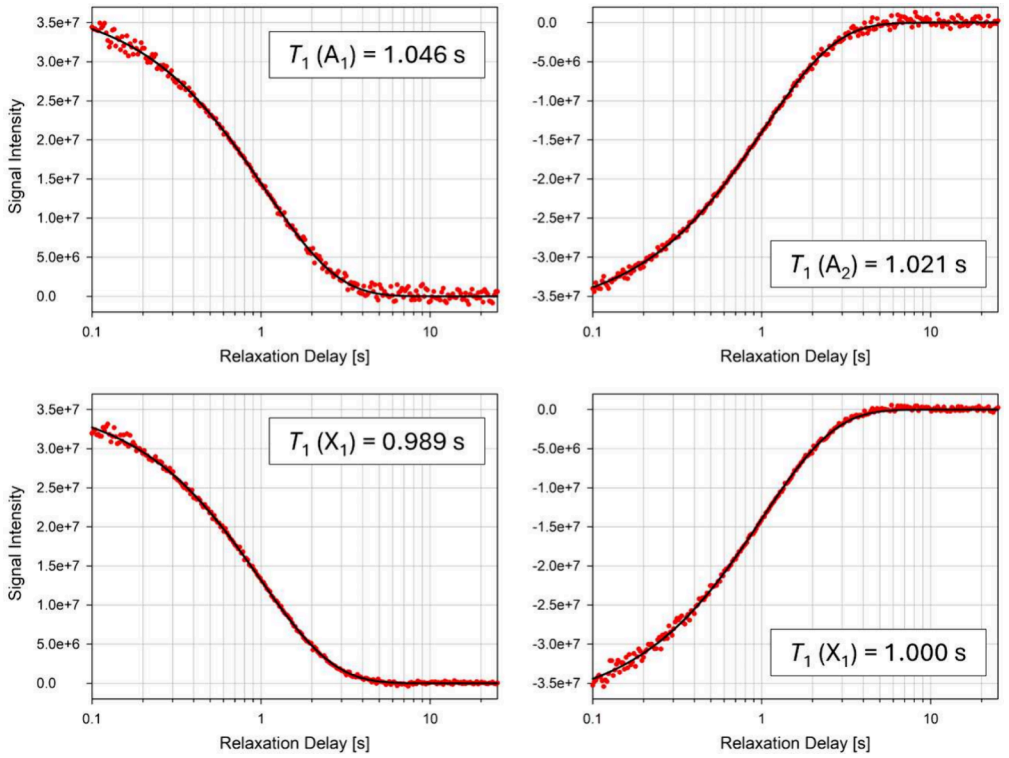

Figure 6. Relaxation plots of antiphase signal intensities of the *trans*-cinnamic acid *trans*-vicinal protons (H_A and H_X) as a function of relaxation delay. The ^{1}H NMR signals were obtained using the newly developed pulse sequence designed to monitor the relaxation of the $2I_{1z}I_{2z}$ spin order and integrated over a 16 Hz (0.04 ppm) range centered around each resonance. Shown are relaxation plots for A_1, A_2, X_1, and X_2 (as defined in Figure 1). The experimental data (red circles) are overlaid with monoexponential fits (black lines), from which the relaxation time constants T_1 were extracted.

Table 1. Relaxation Time Constants (T_1) from Monoexponential Fits of the Integrated H_A and H_X Signal Intensities in *trans*-Cinnamic Acid, Listed Separately for Each Component (A_1, A_2, X_1, X_2) of the Respective Doublets

Experiment	Spin Operator Dynamics	Eigenvalue	T_1 (A_1) [s][a]	T_1 (A_2) [s][a]	T_1 (X_1) [s][a]	T_1 (X_2) [s][a]
In-phase relaxation	$\frac{dI_{1z}}{dt} + \frac{dI_{2z}}{dt}$	−2	1.330 (± 0.002)	1.896 (± 0.007)	1.354 (± 0.002)	1.328 (± 0.002)
Antiphase relaxation	$\frac{d2I_{1z}I_{2z}}{dt}$	−4	1.046 (± 0.007)	1.021 (± 0.005)	0.989 (± 0.003)	1.000 (± 0.005)

[a]Uncertainties represent standard errors from the curve fits.

by inversion-recovery experiments following the SIP-R protocol, while Figure 6 shows the relaxation of the antiphase signals monitored with the newly developed pulse sequence targeting the $2I_1zI_{2z}$ eigenmode. For each pulse sequence, a series of 256 individual experiments was recorded, with each experiment consisting of four dual-scans (total of eight scans) for signal averaging. The recovery delays (τ) were incremented exponentially, i.e., increased linearly on a logarithmic time scale (log τ) from 0.1 to 25 s. Signal intensities were integrated over a spectral width of 16 Hz (0.04 ppm) centered on each resonance. Relaxation curves are shown separately for the four signals of the H_A and H_X doublets (A_1, A_2, X_1, and X_2 as indicated in Figure 1), with the experimental data points overlaid by monoexponential fits to the integrated intensities of each signal.

Table 1 presents the relaxation time constants obtained from monoexponential fits to the integrated intensities of each individual signal of the H_A and H_X doublets (A_1, A_2, X_1, and X_2 as indicated in Figure 1). The data compare results from the SIP-R experiment, which tracks the relaxation of in-phase magnetization, with those from the newly developed dual-scan experiment designed to monitor the relaxation of antiphase magnetization, i.e., relaxation of the $2I_{1z}I_{2z}$ two-spin order corresponding to the eigenmode with eigenvector $[1\ -1\ -1\ 1]^T$ and eigenvalue −4.

RESULTS AND DISCUSSION

The relaxation times observed for antiphase spin order were consistently measured to be approximately 1.0 s for *trans*-cinnamic acid dissolved in DMSO-d_6. Comparable trends were obtained in deuterated acetone (acetone-d_6) and deuterated water (D_2O), although the absolute values of the relaxation time constants varied with the solvent. In every case, the relaxation times of in-phase magnetization were longer than those of the corresponding antiphase magnetization, typically by a factor of 1.3−1.9. Notably, the in-phase relaxation times differed substantially between H_A and H_X and even between the individual signals (A_1 and A_2) of the H_A doublet. A likely explanation not only for the shorter T_1 but also for the larger integrated intensities of A_1 (by a factor of ∼2.5, see Figure 6) is that the chosen integration window of 0.04 ppm (16 Hz) around the resonance center, though narrow, still includes a substantial contribution from overlapping aromatic proton signals. Consequently, the extracted T_1 for A_1 may primarily

https://doi.org/10.1021/acs.jpca.5c05247
J. Phys. Chem. A XXXX, XXX, XXX−XXX

reflect the relaxation of these aromatic protons rather than H_A. None of the in-phase relaxation time constants reached twice the value of the corresponding antiphase relaxation times, although $T_1(A_2)$ approached this limit (see Table 1).

Additional relaxation mechanisms beyond the simplified matrix model presented in eq 5 may further shorten in-phase relaxation times while still leaving them longer than those of antiphase magnetization. As illustrated in Figure 7, double-

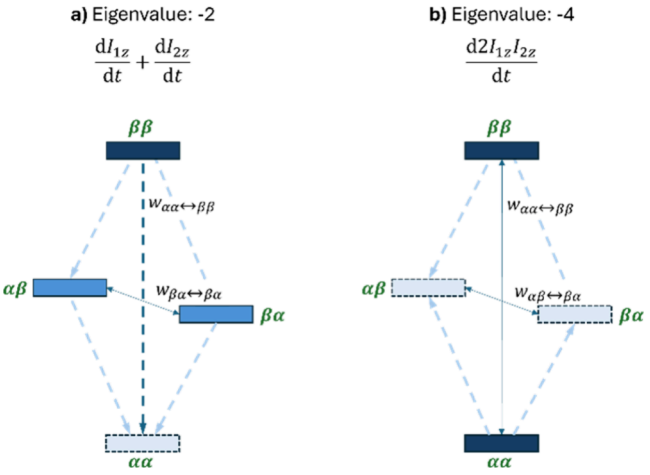

Figure 7. Influence of zero- and double-quantum transitions on the relaxation of (a) in-phase and (b) antiphase magnetization in a weakly coupled two-spin (AX) system. Because of equal populations of the intermediate spin states, zero-quantum transitions between the $\beta\alpha$ and $\alpha\beta$ states (with transition probability $w_{\beta\alpha\leftrightarrow\alpha\beta}$) do not contribute to the relaxation of either in-phase or antiphase magnetization. In contrast, double-quantum transitions between the $\alpha\alpha$ and $\beta\beta$ states (with transition probability $w_{\alpha\alpha\leftrightarrow\beta\beta}$) can accelerate the relaxation of in-phase magnetization but will not affect antiphase magnetization, where the $\alpha\alpha$ and $\beta\beta$ states are equally overpopulated.

quantum relaxation pathways provide one possible explanation. A finite transition probability of $w_{\alpha\alpha\leftrightarrow\beta\beta}$ enables direct exchange between the $\beta\beta$ and $\alpha\alpha$ spin states. This process accelerates the decay of in-phase magnetization but does not affect the two-spin order described by the operator $2I_{1z}I_{2z}$, where the $\beta\beta$ and $\alpha\alpha$ states remain symmetrically overpopulated relative to the equilibrium magnetization. Such pathways therefore selectively enhance in-phase relaxation while leaving antiphase spin order largely unaffected. This observation is consistent with the experimental finding that in-phase relaxation times were always longer than, but never twice as long as, the corresponding antiphase relaxation times.

CONCLUSION

This study demonstrates that antiphase magnetization, whether generated by hyperpolarization techniques or pulse sequences utilizing scalar coupling evolution, can relax substantially faster than in-phase magnetization. Therefore, antiphase relaxation cannot generally be characterized by the conventional T_1 time constant obtained from inversion-recovery or saturation-recovery methods. While theory predicts that antiphase modes may relax up to twice as fast as in-phase modes in a weakly coupled two-spin system, additional mechanisms, such as double-quantum transitions, may accelerate in-phase relaxation while remaining inactive for antiphase spin orders.

For the design of hyperpolarization strategies in NMR and MRI, it is crucial to consider each relaxation mode and its associated eigenvalue independently. It has long been observed, for instance, that PHIP-generated hyperpolarization decays more rapidly than inverted thermal polarization. This study expands the framework for understanding such accelerated decay by introducing the concept that hyperpolarized spin systems may selectively populate intrinsic eigenmodes with larger (i.e., more negative) eigenvalues. An important implication of this study is that future, carefully designed pulse sequences should, at least partially, mitigate relaxation losses by preferentially storing hyperpolarization in modes with smaller eigenvalues such as longitudinal in-phase orders, which are inherently longer-lived than antiphase spin order. Approaches to transfer antiphase to in-phase spin order have been reported previously[23] but without appreciating the associated and potentially beneficial change in relaxation eigenmodes. Developing such strategies with explicit attention to eigenmode relaxation behavior will be an important next step toward extending hyperpolarization lifetimes in both NMR and MRI applications. It is worth noting that storage of hyperpolarization as long-lived singlet states at low magnetic fields represents another strategy to mitigate relaxation losses.[24] However, such an approach does not alter the fundamental observation that in-phase relaxation is inherently slower than antiphase relaxation.

When more than two spins are coupled or the coupling exceeds the weak-coupling limit, relaxation acceleration may become even more pronounced. Preliminary matrix-based calculations for systems of three weakly coupled spin-1/2 nuclei suggest the existence of additional eigenmodes (including one with an eigenvalue of −6) beyond the 0, −2, and −4 eigenvalues observed in two-spin systems.

These findings underscore the need to rethink how relaxation behavior is interpreted in hyperpolarized spin systems. Rather than treating T_1 relaxation as a universal descriptor, a more nuanced approach that accounts for multiple relaxation eigenmodes is required, each with its own distinct lifetimes. As experimental techniques and hyperpolarization strategies continue to evolve, understanding and controlling the specific population modes involved will be critical for optimizing signal lifetimes and maximizing the information extracted from hyperpolarized NMR and MRI experiments.

ASSOCIATED CONTENT

Data Availability Statement

Data will be made available upon request.

AUTHOR INFORMATION

Corresponding Author

Klaus Woelk − *Department of Chemistry, Missouri University of Science and Technology, Rolla, Missouri 65409, United States;* orcid.org/0000-0002-1386-5623; Email: woelk@mst.edu

Authors

Lauren M. Kehoe − *Department of Chemistry, Missouri University of Science and Technology, Rolla, Missouri 65409, United States*

Zachary G. Mayes − *Department of Chemistry, Missouri University of Science and Technology, Rolla, Missouri 65409, United States*

https://doi.org/10.1021/acs.jpca.5c05247
J. Phys. Chem. A XXXX, XXX, XXX−XXX

Kelsey E. Brakensiek − *Department of Chemistry, Missouri University of Science and Technology, Rolla, Missouri 65409, United States*

Emma L. Ellis − *Department of Chemistry, Missouri University of Science and Technology, Rolla, Missouri 65409, United States*

Adam J. Alderfer − *Department of Chemistry, Missouri University of Science and Technology, Rolla, Missouri 65409, United States*

Lingyu Chi − *Department of Chemistry, Missouri University of Science and Technology, Rolla, Missouri 65409, United States*

Complete contact information is available at: https://pubs.acs.org/10.1021/acs.jpca.5c05247

Notes

The authors declare no competing financial interest.

■ ACKNOWLEDGMENTS

The authors acknowledge support from the Missouri S&T Institute for Applied NMR Spectroscopy. This work was supported in part by undergraduate stipends for K.E.B. and E.L.E. through the Opportunity for Undergraduate Research Experience (OURE) program, and for K.E.B. and A.J.A. through the College of Arts, Sciences, and Education (CASE) First Year Research Experience (FYRE) program at Missouri S&T. The authors thank Dr. Martin Bohner (Department of Mathematics and Statistics, Missouri S&T) for his guidance in extracting eigenvalues and eigenvectors from the kinetic equations of the nuclear two-spin systems.

■ REFERENCES

(1) Eills, J.; Budker, D.; Cavagnero, S.; Chekmenev, E. Y.; Elliott, S. J.; Jannin, S.; Lesage, A.; Matysik, J.; Meersmann, T.; Prisner, T.; Reimer, J. A.; Yang, H.; Koptyug, I. V. Spin hyperpolarization in modern magnetic resonance. *Chem. Rev.* **2023**, *123*, 1417−1551.

(2) Pravdivtsev, A. N.; Tickner, B. J.; Glöggler, S.; Hövener, J.-B.; Buntkowsky, G.; Duckett, S. B.; Bowers, C. R.; Zhivonitko, V. V. Unconventional parahydrogen-induced hyperpolarization effects in chemistry and catalysis: From photoreactions to enzymes. *ACS Catal.* **2025**, *15*, 6386−6409.

(3) Kovtunov, K. V.; Pokochueva, E. V.; Salnikov, O. G.; Cousin, S. F.; Kurzbach, D.; Vuichoud, B.; Jannin, S.; Chekmenev, E. Y.; Goodson, B. M.; Barskiy, D. A.; Koptyug, I. V. Hyperpolarized NMR spectroscopy: d-DNP, PHIP, and SABRE techniques. *Chem. An Asian J.* **2018**, *13*, 1857−1871.

(4) Glöggler, S.; Colell, J.; Appelt, S. Para-hydrogen perspectives in hyperpolarized NMR. *J. Magn. Reason.* **2013**, *235*, 130−142.

(5) Green, R. A.; Adams, R. W.; Duckett, S. B.; Mewis, R. E.; Williamson, D. C.; Green, G. G. R. The theory and practice of hyperpolarization in magnetic resonance using parahydrogen. *Progr. NMR Spectrosc.* **2012**, *67*, 1−48.

(6) Buntkowsky, G.; Theiss, F.; Lins, J.; Miloslavina, Y. A.; Wienands, L.; Kiryutin, A.; Yurkovskaya, A. Recent advances in the application of parahydrogen in catalysis and biochemistry. *RSC Adv.* **2022**, *12*, 12477−12506.

(7) Goez, M. Photo-CIDNP spectroscopy. *Annu. Rep. NMR Spectrosc.* **2009**, *66*, 77−147.

(8) Frye, J. S. Comparison of inversion-recovery methods for measuring longitudinal relaxation rates. *Concepts. Magn. Reason.* **1989**, *1*, 27−33.

(9) Kingsley, P. B. Methods of measuring spin-lattice (T_1) relaxation times: An annotated bibliography. *Concepts Magn. Reson.* **1999**, *11*, 243−276.

(10) Keeler, J. Chapter 2 NMR and energy levels: Two Spins. In *Understanding NMR Spectroscopy*; University of Cambridge, 2002.

(11) Keeler, J. Chapter 8 Relaxation: Solomon equations. In *Understanding NMR Spectroscopy*; University of Cambridge, 2002.

(12) Keeler, J. Chapter 8 Relaxation: Rate equations and rate constants. In *Understanding NMR Spectroscopy*; University of Cambridge, 2002.

(13) Woelk, K. Kernresonanzspectroskopische Untersuchungen an chemischen Reaktionen mit spinpolarisiertem Wasserstoff (Nuclear magnetic resonance investigations of chemical reactions with spin-polarized hydrogen). Master's Thesis, University of Bonn, Germany, 1988; pp 26−33.

(14) Mayes, Z. G.; Rice, W. H.; Chi, L.; Woelk, K. A robust Freeman-Hill-inspired pulse protocol for ringdown-free T_1 relaxation measurements. *J. Magn. Reson.* **2023**, *352*, No. 107490.

(15) Mayes, Z. G.; Eriyagama, Y. A. M.; Chi, L.; Schuman, T. P.; Woelk, K. Single and double-selective split-inversion pulse and recovery (SIP-R) sequences for targeted T_1 relaxation measurements. *J. Magn. Reson.* **2025**, *375*, No. 107884.

(16) Bellman, R. E.; Roth, R. S. Numerical Inversion of the Laplace Transform. In *The Laplace Transform*; World Scientific Press, Singapore, 1984.

(17) Fordham, E. J.; Venkataramanan, L.; Mitchell, J.; Valori, A. What are, and what are not, inverse Laplace transforms. *Diffusion Fundamentals* **2017**, *29*, 1.

(18) Donne, D. G.; Gorenstein, D. G. A pictorial representation of product operator formalism: Non-classical vector diagrams for multidimensional NMR. *Concepts Magn. Reson.* **1997**, *9*, 95−111.

(19) Keeler, J. Chapter 6 Product Operators. In *Understanding NMR Spectroscopy*; University of Cambridge, 2002.

(20) McDonald, S.; Warren, W. S. Uses of shaped pulses in NMR: A primer. *Concepts Magn. Reson.* **1991**, *3*, 55−81.

(21) Natterer, J.; Bargon, J. Parahydrogen induced polarization. *Progr. NMR Spectrosc.* **1997**, *31*, 293−315.

(22) Boelens, R.; Podoplelov, A.; Kaptein, R. Separation of net polarization and multiplet effect in coupled spin systems by two-dimensional CIDNP. *J. Magn. Reson.* **1986**, *69*, 116−123.

(23) Sengstschmid, H.; Freeman, R.; Barkemeyer, J.; Bargon, J. A new excitation sequence to observe the PASADENA effect. *J. Magn. Reson. A* **1996**, *120*, 249−257.

(24) Carravetta, M.; Johannessen, O. G.; Levitt, M. H. Beyond the T_1 limit: Singlet nuclear spin states in low magnetic field. *Phys. Rev. Lett.* **2004**, *92*, No. 153003.